Adsorption behavior of methyl orange and methylene blue onto carbon material in an aqueous solution

Yingjie Dai*, Jingjing Li

Laboratory of Environmental Remediation, College of Resources and Environment, Northeast Agricultural University, No. 600 Changjiang Road, Xiangfang District, Harbin 150030, China, Tel. +86 451 5519 0825; Fax: +86 451 5519 0825; emails: dai5188@hotmail.com (Y. Dai), 67384708@qq.com (J. Li)

ABSTRACT

In this research, the adsorptive behavior of carbon materials (CM) derived from the combustion of forest branches was investigated by measuring the removal of organic dyes such as methyl orange (MO) and methylene blue (MB) from an aqueous solution. The influence of parameters such as the adsorption time, pH of the solution, a dose of the adsorbent, and the temperature and adsorption/regeneration cycles of the MO and the MB onto this CM were investigated. The adsorption isotherms of MO and MB on the initial CM were compared with those of an oxidized version (Ox-CM). The results of this work showed that the adsorption ratios of MO and MB on this CM after 3 h were 96.3% and 90.2% at 25°C with the 50 mg/L initial concentrations of dyes and the dose of CM was 0.4 g/L, respectively. The values for this CM were based on the Langmuir isotherm, which showed the parameters for the saturated adsorption amount (Q_0) and the adsorption equilibrium constant (K_L): 285.71 mg/g and 0.1490 L/mg for MO; and, 250.23 mg/g and 0.1360 L/mg for MB, respectively. The adsorption mechanisms can be attributed to the hydrophobic interaction at the interface between the organic dyes and the CM. In the present study, this CM was highly adsorptive of the MO and MB organic dyes.

Keywords: Adsorption isotherm; Carbon material; Hydrophobicity; Kinetics; Organic dyes

1. Introduction

There are more than a hundred thousand types of commercially available dyes with about one million tons of dyestuff produced annually [1,2]. It is suggested that 2% of the dyes produced annually become part of the effluence from manufacturing operations, while 10% is discharged from textile industries [3]. The effluence of dyestuffs in the environment is toxic and harmful to aquatic creatures and can be carcinogenic to humans [4]. Wastewater from industries (such as leather, cosmetics, food coloring, plastics, and printing) contain dyes that should be purified to prevent pollution of the environment. Some techniques have been generally acknowledged for the elimination of dyes from contaminated waters. There are several effective methods for the removal of dyes: photodegradation and biodegradation [5], flocculation [6], membrane separation [7], chemical oxidation [8], electro-coagulation [9], and physical adsorption [10]. Among them, adsorption using activated carbon (AC) has been an effective technique that has shown potential for removing dyes [11], and the removal of dyes onto activated carbon material (CM) has been reported [12–14]. However, commercially available adsorbent material is expensive, such as amberlite Ira-938 [15], nano-metallic particles [16],

---

* Corresponding author.

and modification *Hibiscus cannabinus* fiber [17], and recent research for inexpensive and easily available adsorbents for the removal of dyes from aqueous solutions has focused on abundant materials, require little processing, and are mostly waste material from industry, agriculture, and the forest [18]. A large number of biomass products and other waste materials have been widely used for the adsorption of dyes: the husks of coconuts [19], vermiculata plants [20], date pits [21], olive stones [22], sewage char and tires [23], bamboo dust [24], jute fiber [25], waste apricots [26], corncobs [27], and corn husk [28]. These materials are considered alternative adsorbents due to their low cost and physicochemical properties.

Among low-cost adsorbent materials, CM derived from the combustion of forest branches has previously been reported [29]. Dai et al. [29] prepared this type of CM and commercially available AC to investigate the removal of nitrobenzene (NB) from an aqueous solution. The saturated adsorption amounts of NB were 294 mg/g for CM and 344 mg/g for AC at pH 5.8 and 25°C. However, the adsorption equilibrium constant for CM was about 7 times larger than that of AC. In our previous study, adsorption removal of aromatics compounds such as NB on this CM and AC were investigated, however, there is little information concerning the use of CM to treat dyes-contaminated wastewater in much of the published literature. In addition, the mechanism for the removal in dyes with different charges on CM has not been very clearly elucidated yet. Thus, compared with other previous reports, the study of adsorption behaviors of methyl orange (MO) and methylene blue (MB) onto CM have potential significance to the removal of dyes in wastewater.

The main objective of the present research was to investigate the removal of MO and MB from an aqueous solution using a CM derived from the combustion of forest branches. We investigated the adsorbency of this CM and how it was influenced by adsorption time, the pH of the solution, the dose of the adsorbent, and the temperature of the MO and MB. The adsorption isotherms of the MO and the MB on CM were compared with those of an HNO_3-treated oxidized CM (Ox-CM). Simultaneously, the desorption and regeneration capabilities were evaluated. In addition, adsorption mechanisms of the MO and the MB were decided onto Ox-CM and raw CM. Moreover, further studies on this CM for the removal of organic dyes will be summarized in our next study.
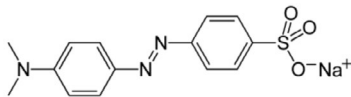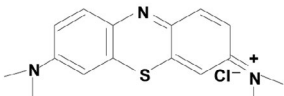
2. Materials and methods

2.1. Materials

Our adsorbent CM was obtained from a power plant that serves Oshu City in Japan. The residue for this CM was derived from the combustion of forest branches that were Japanese cedar and red pine. The wood chips were pyrolyzed at 800°C for 2h. After cooling, the samples are crushed, washed, and dried at 105°C for 24 h to constant weight. To study the effect of the functional groups on the surface of the CM in the removal of dyes, we oxidized a version of the CM with 16 M of nitric acid (10 mL/g CM) at 90°C for 4 h according to a method established by Radovic et al. [30]. After boiling with deionized water and drying at 110°C, the (Ox-CM) was heated at 350°C in air for 4 h to decompose the remaining nitrate ion. The MO and MB were purchased from Wako Pure Chemicals Co., Osaka, Japan. The chemical structures and properties of the MO and MB are shown in Table 1 [31].

2.2. Physical and chemical characteristics of the CM and the Ox-CM

The surface structures of this CM and the Ox-CM version were analyzed using a scanning electron microscopy (SEM) S-3400N (Hitachi Ltd., Tokyo, Japan). The SEM pictures of the CM and the Ox-CM are shown in Fig. 1. These pictures show the surface texture and porosity of the adsorbents. A high porosity and large surface area are essential for highly efficient adsorbents. The SEM picture of the CM displays a partial tubular or rope-like structure, but the surface of Ox-CM shows no such structure due to the oxidization of the nitric acid. The Brunauer–Emmett–Teller (BET) surface area and pore distribution of the CM and the Ox-CM were measured using a surface analyzer, the AUTOSORB 6AG (Yuasa Ionics Co., Osaka, Japan), via the N_2 adsorption method [32,33]. X-ray photoelectron spectroscopy (XPS) was carried out using the XPS/UPS-SPECS System (SPECS Surface Nano Analysis GmbH, Berlin, Germany) to investigate the quantify of carbon-oxygen functional groups. Characterization of the sample surface functional groups was identified by a Fourier transform infrared spectrometer (FTIR, Nicolet 6700, USA) with wavenumbers in the range of 500–4,000 cm^{-1}. The numbers of acidic functional groups and basic sites on the surfaces of the CM and the Ox-CM were determined using an acid-base neutralization method established by Boehm [34]. In a

Table 1
Chemical structure and properties of the targeted dyes

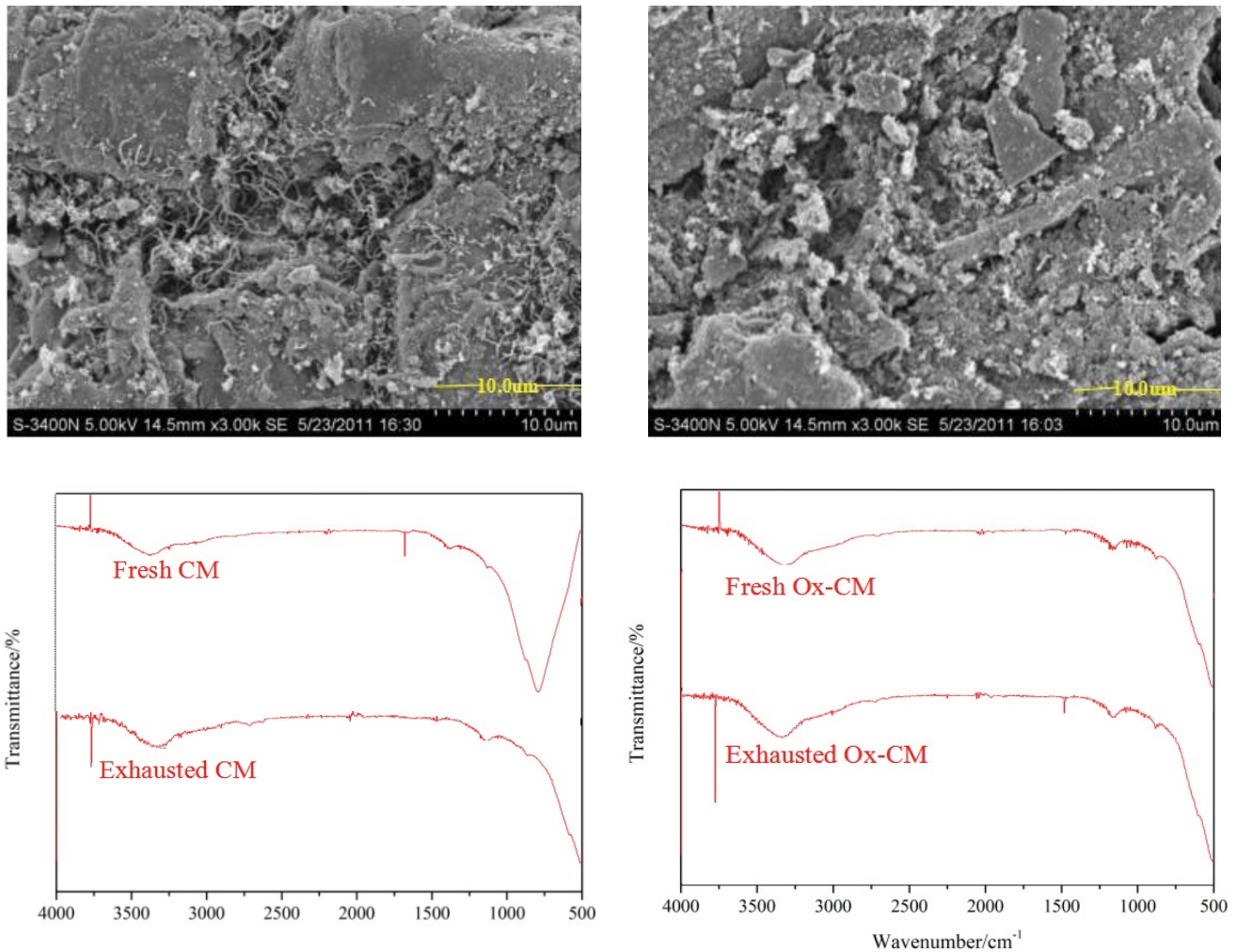| Dyes	Chemical structure	Molecular formula	Molar mass (g/mol)	Charge	Solubility aqueous (g/100 mL)
Methyl orange (MO)		$C_{14}H_{14}N_3O_3S^-Na^+$	327.33	Negative	0.50 (at 20°C)
Methylene blue (MB)		$C_{16}H_{18}N_3S^+Cl^-$	319.86	Positive	3.50 (at 22°C)

Fig. 1. SEM and FTIR images of the CM (left) and the Ox-CM (right).

well-sealed flask, 0.5 g of either CM or Ox-CM with 20 mL of a NaHCO$_3$ (0.1 M), Na$_2$CO$_3$ (0.05 M) or NaOH (0.1 M) solution were mixed to determine the acidity. Then the mixture was further processed by shaking for 48 h at 25°C and 165 rpm. To anti-titrate, each sample, a dose of HCl (0.1 M) was used. NaHCO$_3$ was employed to neutralize only the carboxylic groups on the surface of the CM and the Ox-CM; Na$_2$CO$_3$ was used to neutralize the carboxylic and lactonic groups; and, NaOH was used to neutralize the carboxylic, lactonic and phenolic groups. Accordingly, the groups neutralized by NaHCO$_3$ and Na$_2$CO$_3$ returned lactones, and those neutralized by Na$_2$CO$_3$ and NaOH returned phenolic groups. NaOH (0.1 M) was adopted to titrate the residual base after CM or Ox-CM was exposed to HCl (0.1 M) to determine the basicity. The point of zero charge (pH$_{PZC}$) for both the CM and the Ox-CM was analyzed using a method established by Faria et al. [35]. A 0.01 M NaCl solution was divided evenly into a series of flasks. An adjustment was made to the initial pH (pH$_{initial}$) of from 2.0 to 12.0 by the addition of either HCl (0.1 M) or NaOH (0.1 M). Each flask received a 0.2 g sample of either CM or Ox-CM. Then, the measurement of the mixtures was conducted. The point at which the curve determined by pH$_{final}$ − pH$_{initial}$ crossed the axis, pH$_{initial}$ = pH$_{final}$, represented the pH$_{pzc}$.

2.3. Procedure for the adsorption experiment

The adsorptive features of the adsorbents (CM and Ox-CM) were investigated as a function of adsorption time, pH of the solution, dose of adsorbent, salts, and temperature. The adsorption equilibrium and kinetics were obtained from batch experiments, using 100 mL flasks containing 25 mL of MO and MB solutions and the adsorbents at different temperatures. After equilibrium, the dye solution was separated from the adsorbents via centrifuge at 4,500 rpm for 10 min (IEC61010-2-020, KUBOTA, Japan). The adsorbing amounts of samples were measured using an ultraviolet-visible spectrophotometer V-550 (Jasco Co., Tokyo, Japan) at a wavelength of 463 nm for MO and 665 nm for MB during the time courses. The concentrations of MO and MB were calculated using a standard curve based on the Lambert-Beer law. The dye's amounts on the adsorbents were calculated by the difference between the initial and the equilibrium dyes concentrations in the solution. The removal ratio was calculated

by dividing the number of dyes adsorbed on adsorbents by the initial amount of dyes in the solution. The pH values were achieved using 0.1 M of either HCl or NaOH hourly throughout the experiment. All experiments were performed in triplicate.

2.4. Adsorption kinetics

The controlling mechanism of the adsorption process was investigated using two kinetic models; which were pseudo-first-order and pseudo-second-order models, respectively. The kinetic rate equations can be written as follows

$$\frac{dq_t}{dt} = \left(q_e - q_t\right)^n \tag{1}$$

where q_e and q_t correspond to the amount of MO or MB adsorbed per unit mass of adsorbent (mg/g) at equilibrium and at time t, respectively. k_n is the rate constant for nth-order adsorption (k_n units are 1/min for $n = 1$ and g/mg min for $n = 2$). The linearized integrated forms of the equations are shown as follow,

First-order kinetics ($n = 1$) and second-order kinetics ($n = 2$):

$$\ln\left(q_e - q_t\right) = \ln q_e - k_1 t \tag{2}$$

$$\frac{t}{q_t} = \frac{1}{k_2 q_e^2} + \frac{t}{q_e} \tag{3}$$

The straight-line plots of $\ln(q_e - q_t)$ against t and of t/q_t against t were used to determine the rate constants and correlation coefficients (R^2) for the first and second-order kinetic models, respectively. The fitting equation was selected based on both linear regression R^2 and the calculated q_e values.

Intra-particle diffusion was utilized to explore the rate-controlling steps of the adsorption process. The equation is shown as follow,

$$q_t = k_i t^{0.5} + C \tag{4}$$

where k_i (mg/g min$^{0.5}$) was a rate constant, and C (mg/g) was a constant about the boundary layer thickness.

2.5. Desorption and regeneration experiments

To investigate the recycling of the adsorbents, the dye-loaded adsorbent (CM) following the adsorption of an initial dye concentration of 50 mg/L was regenerated in a 2 M NaCl solution and then was used in another adsorbing test. A more complete regeneration of the adsorbent required 2 M NaCl and 0.05 M NaOH using a method established by Luo and Zhang [31]. To remove the residual NaCl or NaOH, the CM was rinsed slowly with deionized water. The cycle of adsorption–desorption was carried out three times using the same CM and MO (50 mg/L) or MB (50 mg/L). The ratio of the amount of the desorbed dyes to the amount of the adsorbed dyes (MO and MB) represented the efficiency of this CM for the desorption of MO and MB.

3. Results and discussion

3.1. Physical and chemical characteristics of CM and Ox-CM

To compare the surface polarities of the initial form of this CM with those of the Ox-CM version, we measured the acidic and basic functional groups, the BET surface area, the pore size distribution, total pore volume, the pH$_{PZC}$, and the oxygen-containing groups (Table 2). The amount of acidic functional groups on the Ox-CM (1.763 mmol/g) was significantly increased compared with that of the untreated CM (0.063 mmol/g), however, the amount of basic functional groups on the Ox-CM (0.140 mmol/g) was decreased by the nitric acid oxidation. The total BET surface area of the Ox-CM (745 m²/g) was slightly smaller than that of the CM (851 m²/g). The surface areas of the micropores on the CM and the Ox-CM were 597 and 167 m²/g, respectively. The micropore walls of the CM were collapsed, and its mesopores and macropores were extended by the oxidation treatment using a high concentration of nitric acid (16 M). The pH$_{PZC}$ values of the CM and the Ox-CM were 10.7 and 3.8, respectively. Over a wide range of pH, the CM was positively charged; depending on the pH, the Ox-CM was either positive or negative in its surface charge. In Table 2 it can be seen, the oxygen-containing groups of Ox-CM were slightly lower than that of CM. As shown in Fig. 1, the results of FTIR illustrated that the hydroxyl (–OH, 3,791.18 cm^{-1}) appeared after the adsorption of dyes onto CM. And there were no significant differences between fresh Ox-CM and exhausted Ox-CM.

3.2. Adsorption kinetics

We evaluated the contacts between the adsorption ratio of MO and MB and the contact time by shaking 25 mL mixtures of MO (50 mg/L) or MB (50 mg/L) and CM (10 mg)

Table 2
Physical and chemical properties of CM and Ox-CM

	CM	Ox-CM
Acidic functional groups (mmol/g)	0.063	1.763
Carboxylic groups (–COOH)	0.010	0.670
Lactonic groups (–COO–)	0.005	0.160
Phenolic groups (–OH)	0.048	0.930
Basic functional groups (mmol/g)	0.388	0.140
Surface area (m²/g)		
Total (BET surface area)	851	745
Micropore (*t*-plot)	597	167
Meso & macropore (*t*-plot)	254	578
Total pore volume (cm³/g)	0.71	0.63
Average pore size (nm)	4.53	4.26
pH$_{PZC}$	10.70	3.80
Oxygen-containing functional group (At.%)		
C–C, C=C, C–H (284.6 eV)	83.0	77.6
C–O–H, C–O–C (286.2 eV)	8.6	11.6
C=O (287.6 eV)	7.4	7.3
O=C–O (289.2 eV)	1.2	3.6

at 25°C and 165 rpm. Dividing the amount of MO or MB adsorbed onto the CM by the initial amount of MO or MB in the solution produced the adsorption ratio. Fig. 2a shows the effect of contact time on the ratios of MO and MB adsorbed onto the CM. The adsorption ratios of MO and MB on the CM after 3 h were 96.3% and 90.2%, respectively. The removal rates of the MO and the MB were quite fast, within 5 min, but the removal ratio slowly increased and reached equilibrium

at 3 h. This result is important because the equilibrium time is one of the considerations for application to the dyes in a wastewater treatment plant [36].

The controlling mechanism of MO and MB adsorption by CM was investigated by fitting first-order models and second-order models. The results of pseudo-second-order kinetic plots are displayed in Fig. 2b. The parameter in Eqs. (2) and (3), which was determined from kinetic
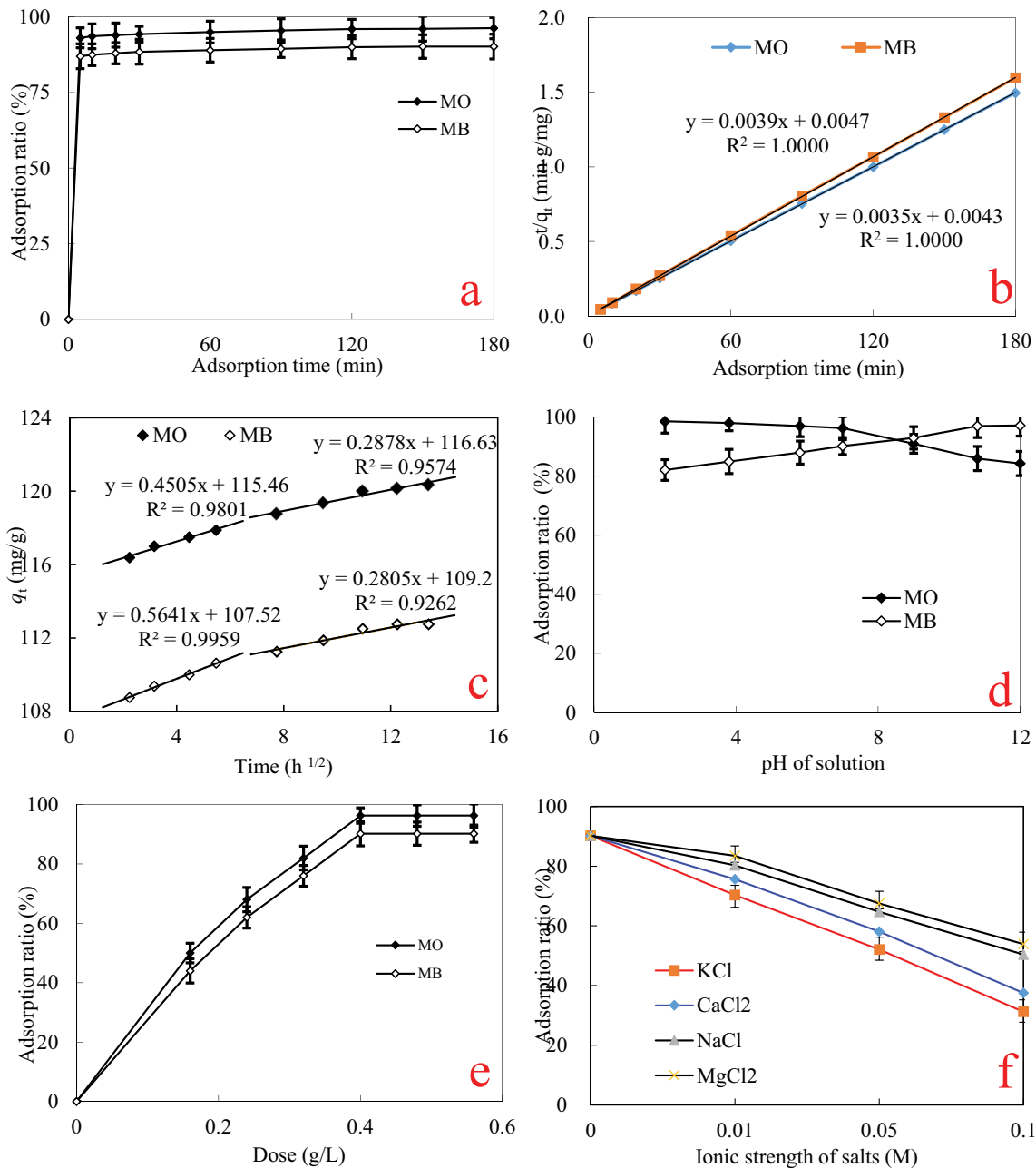

Fig. 2. (a) Effect of adsorption time on MO and MB adsorption by the CM (initial concentration of MO (50 mg/L) and MB (50 mg/L), adsorbent dose = 0.40 g/L, pH = 7.0, at 25°C), (b) pseudo-second-order kinetic plots of MO and MB by the CM, (c) intra-particle diffusion plots of MO and MB by the CM, (d) effect of solution pH on the adsorption of MO and MB by the CM (shaking time 24 h for 25 mL of MO (50 mg/L) and MB (50 mg/L), adsorbent dose = 0.40 g/L, at 25°C), (e) effect of dose on the adsorption of MO and MB by the CM (shaking time 24 h for 25 mL of MO (50 mg/L) and MB (50 mg/L), pH = 7.0, at 25°C), and (f) effect of salts (ionic strength) on the adsorption of MB by the CM (shaking time 24 h for 25 mL of MB (50 mg/L), adsorbent dose = 0.40 g/L, pH = 7.0, at 25°C).

constants of MO and MB on CM are summarized in Table 3. The pseudo-first-order model data do not fall on straight lines. Besides, the calculated q_e values determined from the models differ substantially from those determined experimentally, suggest that the studied adsorption MO and MB on CM is not a pseudo-first-order reaction [37]. On the other hand, the R^2 for the pseudo-second-order kinetic model is equal to 1 (Table 3), and the calculated q_e values (122.16 mg/g for MO and 113.49 mg/g for MB) are acceptable compared to the experimental data (120.38 mg/g for MO and 112.75 mg/g for MB). So, this suggests that the adsorption MO and MB on CM seems to be more of a pseudo-second-order.

The rate-controlling step was explored by the intra-particle diffusion model. The results are shown in Fig. 2c and the parameters are displayed in Table 3. The intra-particle diffusion plots displayed in two steps. In the first step, the adsorbate molecules diffuse from the solution, and the coating liquid film on the surface of the trans-sorbent contacts the surface of the adsorbent, while in the second step, the adsorbate molecules adhere to the surface of the adsorbent through the pore size of the adsorbent. The $k_{i,1}$ and $k_{i,2}$ are the rate parameter of the first step and second step, respectively. Both values of $k_{i,1}$ and $k_{i,2}$ are lower, which indicating that the intra-particle diffusion is regarded as the rate-controlling step of this adsorption process [38,39].

3.3. Effect of the pH of a solution

The pH is an important factor for the adsorption of dyes in some literature [40–42]. The dye adsorption experiments with this CM were carried out using different values for pH (2.0–12.0). The tested samples were prepared by adding the CM (10 mg) to 25 mL of a dye solution when the pH was controlled. Fig. 2d shows the effect of pH on the CM removal of MO and MB from an aqueous solution. The removal ratio of MO decreases as the pH is increasing. When the pH is changed from 2.0 to 12.0, the removal ratio of MO decreased from 98.6% to 84.3%. It may be due to the higher concentration of H+ ions at lower pH values, the negative charges on the surface of CM of internal pores are neutralized and some more new adsorption sites were developed because the surface provided a positive charge attracted to the anionic MO molecules, which enhanced the ability of adsorption for MO onto CM [43]. In contrast, OH⁻ ions caused repulsion between

the negatively charged surface and MO molecules. A similar adsorption behavior was reported by Asuha et al. [44].

On the other hand, the removal ratio of MB increases with the pH increased. It was found that the removal ratio of MB was 82.1% at pH 2.0 and 97.2% at pH 12.0, respectively. The low removal ratio of MB was explained that there are competing between H+ ions and MB cations on the binding-sites of CM surface, thus inhibiting cation dye MB adsorbed at lower pH values. In contrast, it has negatively charged on the surface of CM particles, which enhances the positively charged MB through hydrogen bonds and electrostatic interactions at the pH higher than pH_{PZC} (10.7) [45]. A similar research was observed for MB removal by wood sawdust [46].

3.4. Effect of the adsorbent dose

The adsorbent dose is an important parameter in the removal of dyes via adsorption. The influence of the adsorbent dose on MO and MB adsorption by this CM was estimated. As shown in Fig. 2e, when the adsorbent doses were increased from 0.16 to 0.56 g/L, the percentages of organic dyes adsorbed increased from 50.2% to 96.3% on the CM for MO and from 44.1% to 90.2% for MB. The removal of organic dyes was not increased considerably when the adsorbent doses were higher than 0.4 g/L. The increase in the number of adsorption sites on the surface of the CM was caused by an increase in the total surface area of the CM due to the increase in the adsorbent dose [47]. Thus, the optimum dose of this CM for the adsorption of organic dyes was 0.40 g/ L.

3.5. Effect of the salts for adsorption MB on CM

The influence of the salts such as KCl, $CaCl_2$, NaCl, and $MgCl_2$ were on MB adsorption by this CM was estimated. As shown in Fig. 2f, the removal ratios of MB onto CM were decreased 59.0% for KCl, 52.7% for $CaCl_2$, 39.8% for NaCl and 36.3% for $MgCl_2$, respectively, with the increase of cationic strength from 0 to 0.1 M. The effect of cations on the adsorption capacity of the MB in the solution was: $K^+ > Ca^{2+} > Na^+ > Mg^{2+}$, probably because the cations in the solution occupy the adsorption sites on the surface of CM, and the MB molecule present in the cationic form the competitive adsorption, resulting in that the adsorption amount of MB on CM was decreased [48,49]. There also shows that the

Table 3
Kinetic constants of MO and MB on CM at 25°C

	MO	MB		MO	MB
$q_{e,exp}$ (mg/g)	120.38	112.75	Intra-particle diffusion model		
Pseudo-first-order model			First-step		
k_1 (1/min)	0.0190	0.0216	$k_{i,1}$ (mg/g min$^{0.5}$)	0.451	0.564
q_e (mg/g)	49.24	41.23	C (mg/g)	115.50	107.50
R^2	120.38	0.9568	R^2	0.9801	0.9959
Pseudo-second-order model			Second-step		
k_2 (g/mg min)	0.0028	0.0032	$k_{i,2}$ (mg/g min$^{0.5}$)	0.288	0.281
q_e (mg/g)	122.16	113.49	C (mg/g)	116.60	109.20
R^2	1.0000	1.0000	R^2	0.9570	0.9260

higher cationic strength and valence of salts, on the adsorption of dye the stronger. In addition, the removal ratios of MB in the solution with adding KCl and CaCl$_2$ were less than those of adding NaCl and MgCl$_2$. The reason may be that the hydrated radius of K$^+$ (0.138 nm) and Ca^{2+} (0.123 nm) are larger than those of Na$^+$ (0.102 nm) and Mg^{2+} (0.072 nm), can occupy more adsorption sites on the surfaces of CM, and inhibit the adsorption action for MB [50].

3.6. Adsorption isotherm

Solutions of either MO or MB were used to investigate the effect of temperature on adsorbency. An increase in temperature (10°C–40°C) had a slight influence on the adsorption isotherms of this CM. As indicated in Figs. 3a and b, typical Langmuir-type, Freundlich, Temkin, and Dubinin–Radushkevitch (D–R) pattern were evident in the isothermal curve of organic dyes by both the CM and its Ox-CM version. A linear relationship was observed between the reciprocal of the amount of organic dyes adsorbed onto the CM and the Ox-CM and the reciprocal of the equilibrium concentration of organic dyes in the solution. Tables 4 summarizes the parameters in Eqs. (5)–(11), as determined from the adsorption isotherms of the CM and the Ox-CM:

$$q_e = \frac{Q_0 K_L C_e}{1 + K_L C_e} \tag{5}$$

Here, q_e (mg/g) represents the amount adsorbed; Q_0 (mg/g) is the saturated adsorption amount; K_L (L/mg) is the adsorption equilibrium constant of Langmuir isotherm; and, C_e (mg/L) is the adsorption equilibrium concentration. The amount of dyes adsorbed, q_e (mg/g) was calculated as $q_e = (C_0 − C_e) \times (V/m)$, where C_0 (mg/L), is respectively the initial concentration of the dyes in solution, V (L) the volume of solution and m (g) is the mass of samples.

The Langmuir isotherm is characterized by the Langmuir separation factor (R_L) and is expressed by Eq. (5). The adsorption tends to favor the adsorption equilibrium was judged by the value of R_L [50].

$$R_L = \frac{1}{1 + K_L C_0} \tag{6}$$

The value of R_L, which was in the range of $R_L > 1$, implying an unfavorable adsorption; $R_L = 1$, linear adsorption; $0 < R_L < 1$, favorable adsorption; $R_L = 0$, irreversible adsorption.

$$q_e = K_F C_e^{\frac{1}{n}} \tag{7}$$

where K_F (L/mg) is the empirical constant of Freundlich isotherm associated with adsorption capacity; and the constant n is the empirical parameter related to the adsorption intensity of the adsorbent. When 1/n values are in the range of 0.1–0.5, the adsorption process is favorable [51]. The Freundlich constants were calculated, using the same method as for Langmuir, for a comparison purpose.

The linear equation of the Temkin model is shown as follows,

$$q_e = B \ln K_T + B \ln C_e \tag{8}$$

$$B = \frac{RT}{b_T} \tag{9}$$

where K_T (L/g) is the equilibrium bond constant; B and b_T (J/mol) is the Temkin constant about the sorption heat.

The linear equation of D–R model is shown as follows,

$$\ln q_e = \ln q_m − K_D \varepsilon^2 \tag{10}$$

$$\varepsilon = RT \ln \left(1 + \frac{1}{C_e} \right) \tag{11}$$

where q_m (mg/g) is the maximum adsorption capacity; K_D (mol^2/J^2) is the activity coefficient about the free energy of adsorption and ε is the Polanyi potential.

Compared with the Freundlich isotherm model and D–R isotherm model, the Langmuir isotherm model, and Temkin isotherm model yielded a higher correlation coefficient, which was higher than 0.95. Consequently, the Langmuir isotherm and Temkin fitted the experimental data well, which illuminated that the adsorption mechanism was involved
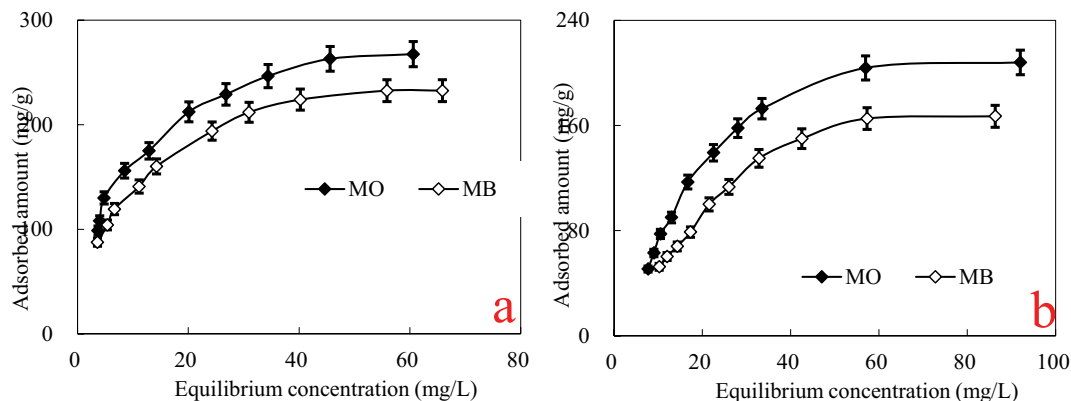

Fig. 3. (a) Adsorption isothermal curve of MO and MB by the CM and (b) adsorption isothermal curve of MO and MB by the Ox-CM (shaking time 24 h for 25 mL of MO (10 to 200 mg/L) and MB (10–200 mg/L), adsorbent dose = 0.40 g/L, pH = 7.0, at 25°C).

in the dyes adsorption process, the surface adsorption sites and adsorption energies of adsorbent were homogenous in its distribution. What's more, the adsorption process is a chemisorption process that adsorption heat decreases linearly with changes in performance coverage. Since the experimental data does not fit to the D–R isotherm model, which indicates that the adsorption process is not dominated by the pore-filling mechanism. In addition, in this work, the values of Langmuir separation factors (R_L), which were in the range of 0.03–0.74 for all cases, showing favorable adsorption of dyes onto the CM and the Ox-CM [52].

Table 4 shows the values of the parameters obtained for the CM from the Langmuir isotherm: Q_0 and K_L were 285.71 mg/g, 0.1490 L/mg for MO and 250.23 mg/g, and 0.1360 L/mg for MB. On the other hand, the results on the adsorption of MO and MB by the Ox-CM showed that Q_0 and K_L were 204.08 mg/g, 0.0400 L/mg for MO and 172.41 mg/g, and 0.0360 L/mg for MB (Table 4). The total BET surface area of the CM (851 m²/g) was slightly larger than that of the Ox-CM (745 m²/g). However, the values for the Q_0 of the CM for MO and MB were about 1.5 times larger than those of the Ox-CM version. The surface hydrophobic interaction of the CM was greater than that of the Ox-CM, as described in section 3.7, because of a stronger interaction between the adsorbent (CM) and the adsorbing molecules (MO or MB). The results obtained using our CM were superior to those of other adsorbents reported in the literature [21,53–64] (Table 5): living biomass (1.17 mg/g), activated date pits (17.30 mg/g), coconut husk-based AC (66.00 mg/g), activated sewage char (120.00 mg/g), and saw dust (133.87 mg/g).

3.7. Adsorption mechanism of MO and MB

The removal of a harmful substance onto an adsorbent depends on various surface factors, such as functional groups, surface area and pore size distribution [65]. A test was performed using the Ox-CM to examine the effect of the functional groups after the oxidation of a CM. There were approximately 128 fewer acidic functional groups on

the surface of the initial version of this CM (0.063 mmol/g) than on the surface of its Ox-CM version (1.763 mmol/g) (Table 2). In these results, the Q_0 and K_L for both MO and MB were largely decreased in the Ox-CM (Table 4). This happened because the functional groups on the surface weakened the hydrophobic properties of the CM, which translated to a decrease in the Q_0 and K_L of the Ox-CM. Surface hydrophobicity is an important factor for an adsorptive

Table 4
Parameters of adsorption isotherms of MO and MB on CM and Ox-CM at 25°C

Adsorbents	CM		Ox-CM	
Samples	MO	MB	MO	MB
Langmuir isotherm				
Q_0 (mg/g)	285.71	250.23	204.08	172.41
K_L (L/mg)	0.1490	0.1360	0.0400	0.0360
R^2	0.9931	0.9944	0.9907	0.9914
R_L	0.03–0.40	0.04–0.42	0.11–0.71	0.12–0.74
Freundlich isotherm				
K_F (L/mg)	69.45	60.05	19.76	14.74
$1/n$	0.3521	0.3480	0.5789	0.5934
R^2	0.9690	0.9725	0.8992	0.9301
Temkin isotherm				
K_T (L/g)	1.496	1.349	0.303	0.232
b_T (J/mol)	61.352	54.274	69.037	61.359
R^2	0.9916	0.9878	0.9664	0.9639
D–R isotherm				
q_m (mg/g)	231.00	198.60	180.90	148.60
K_D (mg²/KJ²)	3×10^{-6}	3×10^{-6}	2×10^{-5}	2×10^{-5}
R^2	0.8958	0.7940	0.9444	0.9066

Table 5
Maximum uptake capacity for the adsorption of MB onto various adsorbents

Adsorbents	Uptake capacity (mg/g)	References
Fe₃O₄@AMCA-MIL-53(Al) nanocomposite	325.62	[53]
Multi-walled carbon nanotubes	178.5	[54]
Bagasse bottom ash	142.54	[55]
Saw dust	133.87	[56]
Activated sewage char (800°C)	120.00	[57]
Activated carbon prepared from a renewable bio-plant of *Euphorbia rigida*	109.98	[58]
Composite material	74.00	[59]
Coconut husk based activated carbon	66.00	[60]
Activated *Rosa canina* seeds (500°C)	47.20	[61]
Activated lignin-chitosan extruded blends	36.25	[62]
Activated date pits (900°C)	17.30	[21]
Cobalt–zinc ferrite nanoadsorbent	3.40	[63]
Living biomass	1.17	[64]
Carbon material prepared from the combustion of forest branches	250.23	This study

organic compound [66]. As shown in Table 2, there were fewer acidic functional groups on the surface of the initial version of this CM. Therefore, the surface polarity of this CM was very low, which strengthened the hydrophobic properties compared with those of the Ox-CM version. The strong hydrophobicity of the CM surface explained the high K_L for MO and MB. When an aqueous solution is used as the solvent, a low hydrophobicity of an adsorbent surface reduces the adsorptive capacity. The solubility of the aqueous MO (0.5 g/100 mL, at 20°C) was lower than that of the MB (3.5 g/100 mL, at 22°C) [31], therefore, the Q_0 and K_L values of the MO were greater on this CM than those of the MB, because the hydrophobicity of the MO was greater. In order to achieve high efficiency, a moderately water-soluble substance, such as MO and MB, requires that the adsorbent have strong hydrophobic properties.

In addition, Cπ-cation interactions are primary owing to the electrostatic interplay between the cation dye and the quadrupole moment of the graphene layers on the surface of CM [67]. The adsorption capacity of the MB cation dye was decreased after the CM was oxidized. The reasons are as follows: The oxygen-containing functional groups on the surface of oxidized CM are electron withdrawals groups. The π electron density on the Ox-CM skeleton was weakened by these oxygen-containing functional groups. Thereby weakening the π–π effect between the adsorbent and the adsorbate, resulting in decreased adsorption capacity of the MB cation dye on Ox-CM.

3.8. Desorption and regeneration

The regenerative functions of this CM are summarized in Fig. 4 and Table 6. The results show three adsorption/regeneration cycles for the CM, and the adsorbed dyes were mostly released after regeneration, while the capacity for dye adsorption remained unchanged. The adsorptive capacity was regained after three cycles of adsorption and elution,

Table 6
Regenerative functions of the CM

Recycling times	1	2	3
MO (adsorption ratios, %)	96.30	95.80	95.20
MB (adsorption ratios, %)	90.20	89.80	89.30

and desorption efficiency remained at approximately 90% for both MO and MB. The results of this study showed that this CM can be regenerated and reused many times.

4. Conclusions

We used aqueous solutions of MO and MB to examine the adsorptive capacity of a CM derived from the combustion of forest branches. The following conclusions can be drawn:

- The removal ratio of MO decreases as the pH is increasing, however, that of MB increases with the pH increased.
- An increase in temperature had a slight influence on the adsorption isotherms of this CM.
- Three adsorption/regeneration cycles for the CM and the adsorbed dyes were mostly released after regeneration, while the capacity for dye adsorption remained unchanged from 96.30% to 95.20% for MO and 90.20% to 89.30% for MB, respectively.
- Adsorption mechanisms contributed to the hydrophobic interactions that occurred at the interface between the organic dyes and the CM.
- The maximum adsorption capacity of CM to MB and MO were 250.23 and 285.71 mg/g at 25°C with the 50 mg/L initial concentrations of dyes and the 0.40 g/L of adsorbent dose.

The present study shows that CM derived from the combustion of forest branches can be an inexpensive and effective adsorbent for the removal of organic dyes such as MO and MB from aqueous solutions.
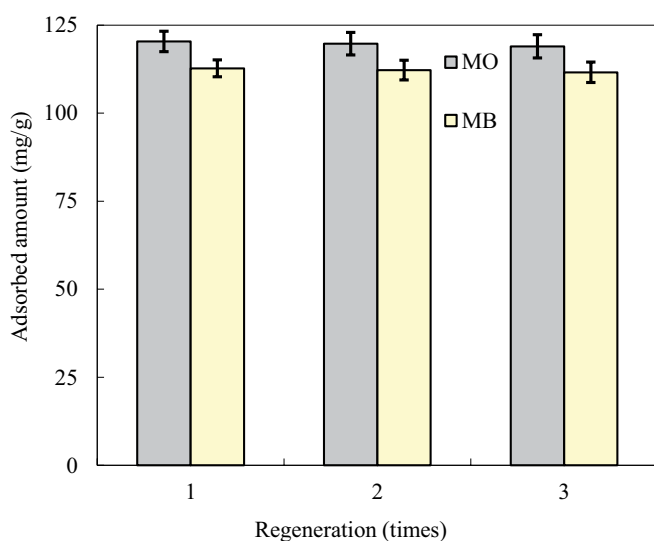
Fig. 4. Three cycles of adsorption/desorption for MO and MB by the CM (shaking time 24 h for 25 mL of MO (50 mg/L) and MB (50 mg/L), adsorbent dose = 0.40 g/L, pH = 7.0, at 25°C).

References

[1] C.I. Pearce, J.R. Lloyd, J.T. Guthrie, The removal of colour from textiles wastewater using whole bacterial cells: a review, Dyes Pigm., 58 (2003) 179–196.
[2] J.W. Lee, S.P. Choi, R. Thiruvenkatachai, W.G. Shim, H. Moon, Evaluation of the performance of adsorption and coagulation

processes for the maximum removal of reactive dyes, Dyes Pigm., 69 (2006) 196–203.

[3] S. Zhao, T. Zhou, Biosorption of methylene blue from wastewater by an extraction residue of *Salvia miltiorrhiza Bge*, Bioresour. Technol., 219 (2016) 330–337.

[4] H. Metivier-Pignon, C. Faur-Brasquet, P.L. Cloirec, Adsorption of dyes onto activated carbon cloths: approach of adsorption mechanisms and coupling of AC with ultra filtration to treat coloured wastewaters, Sep. Purif. Technol., 31 (2003) 3–11.

[5] J. Yener, T. Kopac, G. Dogu, T. Dogu, Adsorption of basic yellow 28 from aqueous solutions with clinoptilolite and amberlite, J. Colloid Interface Sci., 294 (2006) 255–264.

[6] X. Tan, S. Liu, Y. Liu, Y. Gu, G. Zeng, X. Hu, X. Wang, S. Liu, L. Jiang, Biochar as potential sustainable precursors for activated carbon production: multiple applications in environmental protection and energy storage, Bioresour. Technol., 227 (2017) 359–372.

[7] S. Pal, A.S. Patra, S. Ghorai, A.K. Sarkar, V. Mahato, S. Sarkar, R.P. Singh, Efficient and rapid adsorption characteristics of templating modified guar gum and silica nanocomposite toward removal of toxic reactive blue and Congo red dyes, Bioresour. Technol., 191 (2015) 291–299.

[8] M. Muthukumar, N. Selvakumar, Studies on the effect of inorganic salts on decolouration of acid dye effluents by ozonation, Dyes Pigm., 62 (2004) 221–228.

[9] A. Alinsafi, M. Khemis, M.N. Pons, J.P. Leclerc, A. Yaacoubi, A. Benhammou, A. Nejmeddine, Electro-coagulation of reactive textile dyes and textile wastewater, Chem. Eng. Process., 44 (2005) 461–470.

[10] I.D. Mall, V.C. Srivastava, N.K. Agarwal, I.M. Mishra, Removal of congo red from aqueous solution by bagasse fly ash and activated carbon: kinetic study and equilibrium isotherm analyses, Chemosphere, 61 (2005) 492–501.

[11] K. Jung, B. Choi, M. Hwang, T. Jeong, K. Ahn, Fabrication of granular activated carbons derived from spent coffee grounds by entrapment in calcium alginate beads for adsorption of acid orange 7 and methylene blue, Bioresour. Technol., 219 (2016) 185–195.

[12] L.L. Prasanna, S. Jiwan, C. Jong-Soo, C. Yoon-Young, Y. Jae-Kyu, K.R. Rao, Multivariate modeling via artificial neural network applied to enhance methylene blue sorption using graphene-like carbon material prepared from edible sugar, J. Mol. Liq., 265 (2018) 416–427.

[13] L.L. Prasanna, C. Jong-Soo, Y. Jae-Kyu, Adsorption removal of selected anionic and cationic dyes by using graphitic carbon material prepared from edible sugar: a study of kinetics and isotherms, Acta Chim. Slov., 65 (2018) 599–610.

[14] C. Jong-Soo, K.J. Reddy, L.L. Prasanna, Y. Jae-kyu, C. Yoon-Young, Effective adsorptive removal of 2,4,6-trinitrotoluene and hexahydro-1,3,5-trinitro-1,3,5-triazine by pseudographitic carbon: kinetics, equilibrium and thermodynamics, Environ. Chem., 15 (2018) 100–112.

[15] M. Naushad, Z.A. Alothman, M.R. Awual, S.M. Alfadul, T. Ahamad, Adsorption of rose Bengal dye from aqueous solution by amberlite Ira-938 resin: kinetics, isotherms, and thermodynamic studies, Desal. Wat. Treat., 57 (2019) 13527–13533.

[16] S. Jiwan, C. Yoon-Young, R.K. Janardhan, Y. Jae-kyu, Potential degradation of methylene blue (MB) by nano-metallic particles: a kinetic study and possible mechanism of MB degradation, Environ. Eng. Res., 23 (2018) 1–9.

[17] G. Sharma, M. Naushad, D. Pathania, A. Mittal, G.E. El-de-soky, Modification of *Hibiscus cannabinus* fiber by graft copolymerization: application for dye removal, Desal. Wat. Treat., 54 (2015) 3114–3121.

[18] M. Rafatullah, O. Sulaiman, R. Hashim, A. Ahmad, Adsorption of methylene blue on low-cost adsorbents: a review, J. Hazard. Mater., 177 (2010) 70–80.

[19] I.A.W. Tan, A.L. Ahmad, B.H. Hameed, Adsorption of basic dye on high-surface-area activated carbon prepared from coconut husk: equilibrium, kinetic and thermodynamic studies, J. Hazard. Mater., 154 (2008) 337–346.

[20] B. Bestani, N. Benderdouche, B. Benstaali, M. Belhakem, A. Addou, Methylene blue and iodine adsorption onto an activated desert plant, Bioresour. Technol., 99 (2008) 8441–8444.

[21] F. Banat, S. Al-Asheh, L. Al-Makhadmeh, Evaluation of the use of raw and activated date pits as potential adsorbents for dye containing waters, Process Biochem., 39 (2003) 193–202.

[22] M. Alaya, M. Hourieh, A. Youssef, F. El-Sejarah, Adsorption properties of activated carbons prepared fromolive stones by chemical and physical activation, Adsorpt. Sci. Technol., 18 (1999) 27–42.

[23] Y. Lin, H. Teng, Mesoporous carbons from waste tire char and their application in wastewater discoloration, Microporous Mesoporous Mater., 54 (2002) 167–174.

[24] B.H. Hameed, A.T.M. Din, A.L. Ahmad, Adsorption of methylene blue onto bamboo-based activated carbon: kinetics and equilibrium studies, J. Hazard. Mater., 141 (2007) 819–825.

[25] S. Senthilkumaar, P.R. Varadarajan, K. Porkodi, C.V. Subbhuraam, Adsorption of methylene blue onto jute fiber carbon: kinetics and equilibrium studies, J. Colloid Interface Sci., 284 (2005) 78–82.

[26] C.A. Basar, Applicability of the various adsorption models of three dyes adsorption onto activated carbon prepared waste apricot, J. Hazard. Mater., B, 135 (2006) 232–241.

[27] R.L. Tseng, S.K. Tseng, F.C. Wu, Preparation of high surface area carbons from corncob using KOH combined with CO_2 gasification for the adsorption of dyes and phenols from water, Colloids Surf., A, 279 (2006) 69–78.

[28] S. Mishra, S.S. Yadav, S. Rawat, J. Singh, J.R. Koduru, Corn husk derived magnetized activated carbon for the removal of phenol and para-nitrophenol from aqueous solution: interaction mechanism, insights on adsorbent characteristics, and isothermal, kinetic and therodynamic properties, J. Environ. Manage., 246 (2019) 362–373.

[29] Y. Dai, Y. Mihara, S. Tanaka, K. Watanabe, N. Terui, Nitrobenzene-adsorption capacity of carbon materials released during the combustion of woody biomass, J. Hazard. Mater., 174 (2010) 776–781.

[30] L.R. Radovic, I.F. Silva, J.I. Ume, J.A. Menéndez, C.A.L. Leon, A.W. Scaroni, An experimental and theoretical study of the adsorption of aromatics possessing electron-withdrawing and electron-donating functional groups by chemically modified activated carbons, Carbon, 35 (1997) 1339–1348.

[31] X. Luo, L. Zhang, High effective adsorption of organic dyes on magnetic cellulose beadsentrapping activated carbon, J. Hazard. Mater., 171(2001) 340–347.

[32] B.C. Lippens, J.H.D. Boer, Studies on pore systems in catalysts. V The *t* method, J. Catal., 4 (1965) 319–323.

[33] J.H.D. Boer, B.G. Linsen, T.V.D. Plas, G.J. Zondervan, Studies on pore systems in catalysts VII. Description of the pore dimensions of carbon blacks by the *t* method, J. Catal., 4 (1965) 649–653.

[34] H.P. Boehm, Surface oxides on carbon and their analysis: a critical assessment, Carbon, 40 (2002) 145–149.

[35] P.C.C. Faria, J.J.M. Orfao, M.F.R. Pereira, Adsorption of anionic and cationic dyes on activated carbons with different surface chemistries, Water Res., 38 (2004) 2043–2052.

[36] V. Rocher, J.M. Siaugue, V. Cabui, A. Bee, Removal of organic dyes by magnetic alginate beads, Water Res., 42 (2008) 1290–1298.

[37] A.A. Alqadami, M. Naushad, M.A. Abdalla, M.R. Khan, Z.A. Alothman, Adsorptive removal of toxic dyr using Fe_3O_4-TSC nanocomposite: equilibrium, kinetic, and thermodynamic studies, J. Chem. Eng. Data, 61 (2016) 3806–3813.

[38] A.A. Alqadami, M. Naushad, Z.A. Alothman, A.A. Ghfar, Novel metal-organimc framework (MOF) based composite material for the sequestration of U(VI) and Th(IV) metal ions from aqueous environment, ACS Appl. Mater. Interfaces, 9 (2017) 36026–36037.

[39] Y. Zhou, X. Liu, Y. Xiang, P. Wang, J. Zhang, F. Zhang, J. Wei, L. Luo, M. Lei, L. Tang, Modification of biochar derived from sawdust and its application in removal of tetracycline and copper from aqueous solution: adsorption mechanism and modeling, Bioresour. Technol., 245 (2017) 266–273.

[40] L. Wang, J. Zhang, A. Wang, Fast removal of methylene blue from aqueous solution by adsorption onto chitosan-*g*-poly (acrylic acid)/attapulgite composite, Desalination, 266 (2011) 33–39.

[41] W. Chen, L. Duan, D. Zhu, Adsorption of polar and nonpolar organic chemicals to carbon nanotubes, Environ. Sci. Technol., 41 (2007) 8295–8300.

[42] N.K. Lazaridis, G.Z. Kyzas, A.A. Vassiliou, D.N. Bikiaris, Chitosan derivatives as biosorbents for basic dyes, Langmuir, 23 (2007) 7634–7643.

[43] O. Hamdaoui, E. Naffrechoux, Modeling of adsorption isotherms of phenol and chlorophenols onto granular activated carbon: Part II. Models with more than two parameters, J. Hazard. Mater., 147 (2007) 401–411.

[44] S. Asuha, X.G. Zhou, S. Zhao, Adsorption of methyl orange and Cr(VI) on mesoporous TiO_2 prepared by hydrothermal method, J. Hazard. Mater., 181 (2010) 204–210.

[45] B.H. Hameed, Equilibrium and kinetic studies of methyl violet sorption by agricultural waste, J. Hazard. Mater., 154 (2008) 204–212.

[46] A.E. Ofomaja, Kinetic study and sorption mechanism of methylene blue and methyl violet onto mansonia (*Mansonia altissima*) wood sawdust, Chem. Eng. J., 143 (2008) 85–95.

[47] X. Wang, J. Lu, B. Xing, Sorption of organic contaminants by carbon nanotubes: influence of adsorbed organic matter, Environ. Sci. Technol., 42 (2008) 3207–3012.

[48] Y. Gao, Y. Li, L. Zhang, H. Huang, J. Hu, S.M. Shah, X. Su, Adsorption and removal of tetracycline antibiotics from aqueous solution by graphene oxide, J. Colloid Interface Sci., 368 (2012) 540–546.

[49] L. Ji, Y. Shao, Z. Xu, S. Zheng, D. Zhu, Adsorption of monoaromatic compounds and pharmaceutical antibiotics on carbon nanotubes activated by KOH etching, Environ. Sci. Technol., 44 (2010) 6429–6436.

[50] N. Boujelben, J. Bouzid, Z. Elouear, M. Feki, F. Jamoussi, A. Montiel. Phosphorus removal from aqueous solution using iron coated natural and engineered sorbents, J. Hazard. Mater., 151 (2008) 103–110.

[51] R. Mallampati, S. Valiyaveettil, Apple peels-a versatile biomass for water purification, ACS Appl. Mater. Interfaces, 5 (2013) 4443–4449.

[52] D.B. Mckay, I.T. Weber, T.A. Steitz, Structure of catabolite activator protein at 2.9 Å resolution, J. Biol. Chem., 257 (1982) 9518–9524.

[53] A.A. Abdullah, M. Naushad, Z.A. Alothman, T. Ahamad, Adsorptive performance of MOF nanocomposite for methylene blue and malachite green dyes: kinetics, isotherm and mechanism, J. Environ. Manage., 223 (2018) 29–36.

[54] T. Ahamad, M. Naushad, G.E. Eldesoky, S.I. Al-Saeedi, A. Nafady, N.S. Al-Kadhi, A.H. Al-Muhtaseb, A.A. Khan, A. Khan, Effective and fast adsorptive removal of toxic cationic dye (MB) from aqueous medium using amino-functionalized magnetic multiwall carbon nanotubes, J. Mol. Liq., 282 (2019) 154–161.

[55] K.V. Kumar, Adsorption isotherm for basic dye onto low cost adsorbents, Res. J. Chem. Environ., 6 (2002) 61–65.

[56] S. Hakraborty, S. De, S. Dasgupta, J.K. Basu, Removal of Dyes from Aqueous Solution Using a Low Cost Adsorbent, Water and Wastewater Perspectives of Developing Countries, Proceedings of International Conference, International Water Association, New Delhi India, 2002, pp. 1089–1096.

[57] C. Saniz-Diaz, A. Griffiths, Activated carbon from solid wastes using a pilot-scale batch flaming pyrolyser, Fuel, 79 (2000) 1863–1871.

[58] O. Gercel, A. Ozcan, A.S. Ozcan, H.F. Ercel, Preparation of activated carbon from a renewable bio-plant of *Euphorbia rigida* by H_2SO_4 activation and its adsorption behavior in aqueous solutions, Appl. Surf. Sci., 253 (2007) 4843–4852.

[59] V.J.P. Vilar, C.M.S. Botelho, R.A.R. Boaventura, Methylene blue adsorption by algal biomass based materials: biosorbents characterization and process behavior, J. Hazard. Mater., 147 (2007) 120–132.

[60] H. Tamai, T. Kakii, Y. Hirota, T. Kumamoto, H. Yasuda, Synthesis of extremely large mesoporous activated carbon and its unique adsorption for giant molecules, Chem. Mater., 8 (1996) 454–462.

[61] A. Gurses, C. Dogar, S. Karaca, M. Acikyildiz, R. Bayrak R, Production of granular activated carbon from waste *Rosa canina* sp. seeds and its adsorption characteristics for dye, J. Hazard. Mater., B131 (2006) 254–259.

[62] A.B. Albadarin, M.N. Collins, N. Mu, S. Shirazian, G. Walker, C. Mangwandi, Activated lignin-chitosan extruded blends for efficient adsorption of methylene blue, Chem. Eng. J., 307 (2016) 264–272.

[63] T. Tetiana, P. Natalia, N. Bitra, R. Babu, Adsorptive removal of toxic methylene blue and acid orange 7 dyes from aqueous medium using cobalt-zinc ferrite nanoadsorbents, Desal. Wat. Treat., 150 (2019) 374–385.

[64] Y. Fu, T. Viraraghavan, Removal of a dye from an aqueous solution by the fungus *Aspergillus niger*, Water Qual. Res. J. Can., 35 (2000) 95–111.

[65] Y. Feng, Y. Liu, L. Xue, H. Sun, Z. Guo, Y. Zhang, L. Yang, Carboxylic acid unctionalized sesame straw: a sustainable cost-effective bioadsorbent with superior dye adsorption capacity, Bioresour. Technol., 238 (2017) 675–683.

[66] R. Voss, *Mesoporous Organosilica* Materials with Amine Functions: Surface Characteristics and Chirality, Ph.D. Dissertation, Potsdam University, 2005, pp. 83–92.

[67] D.A. Dougherty, Cation-π interactions in chemistry and biology: a new view of benzene, Phe, Tyr, and Trp, Science, 271 (1996) 163–168.